24nm Pr^{3+}:BaY_2F_8 crystal nanoparticles produced by high-energy ball milling: spectroscopic characterization and comparison with bulk properties.

R. Hakim[a], K. Damak[b], M. Gemmi[c], S. Luin[d], R. Maalej[e] , A.Toncelli[f]

[a] Laboratory of Industrial Chemistry, Sfax University, ENIS 3038 Sfax, Tunisia.

[b] Laboratory of Radio Analysis and Environment, Sfax University, ENIS, 3038 Sfax, Tunisia.

[c] Center for Nanotechnology Innovation@NEST, Istituto Italiano di Tecnologia, Piazza S Silvestro 12 56127, Pisa, Italy.

[d] NEST, Scuola Normale Superiore and Istituto Nanoscienze – CNR, Piazza S Silvestro 12 56127, Pisa, Italy.

[e] Laboratoire Géoressouces, Matériaux, Environnement et Changements Globaux, Faculté des Sciences de Sfax, Université de Sfax, 3018 Sfax, Tunisia.

[f] NEST-Istituto Nanoscienze - CNR, University of Pisa, Physics Department “Enrico Fermi”, Largo B.Pontecorvo, 3-Pisa 56127, Italy.

Graphical Abstract

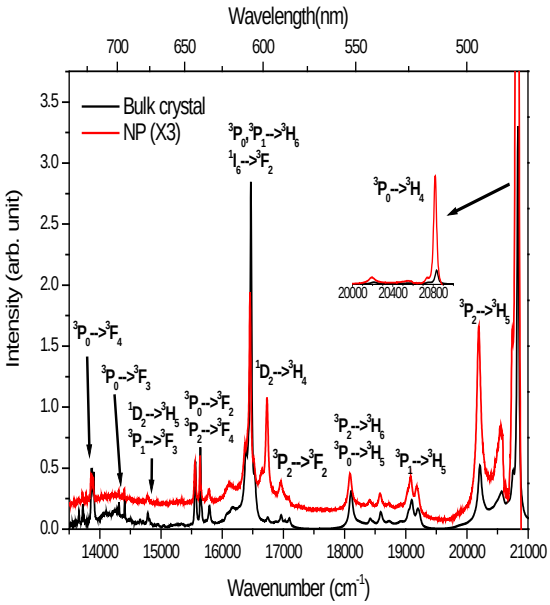

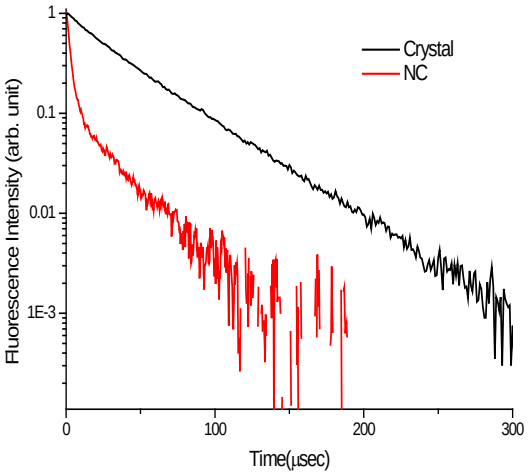

Abstract

Nanocrystals (NC) of Pr^{3+}:BaY_2F_8 with average diameter of 24nm have been successfully prepared by high-energy ball milling. The method is versatile, easily scalable and does not require the use of surfactants or catalysts. NC were prepared starting from high quality single crystal pieces and their spectroscopic features are analyzed and compared with those of a single bulk crystal. Under 445nm excitation, we recorded the 10K and room temperature emission spectra of the two samples. The spectra show the same peak positions and width, and this means that the milling process does not introduce substantial modifications to the crystal structure. Besides, there are strong differences in the relative intensity of the lines emitted towards different lower lying levels in the two samples. In particular the high-energy transitions seem to be hyper intense in the NC with respect to the bulk sample. On the contrary, the emission lines that ends at excited levels are less intense in the NC. In addition, the time evolution of the $^3P_0$ decay shows striking differences between the nano-sized materials and the bulk sample. Despite the exponential decay of the latter luminescence (τ=43μsec), NC possess a strong non linear component with a lifetime much shorter than in the bulk. Calculations show that nearly 89% of the excited ions contribute to the short-time decay, which is attributed to ions residing near the NP surface.

1. Introduction

Lanthanide-doped nanoparticles have gained considerable attention thanks to their high potential in a wide range of photonic applications, such as photoelectric devices [1-2], liquid lasers [3], nano-labels in biological imaging [4-5] or in nanomedicine [6-7]. Among them, rare earth-doped fluoride nanocrystals (NC) possess unique spectral features [8-10] that make them interesting for several applications. Fluoride NC are considered non-toxic and the large choice of dopants and doping levels permits to tailor the emission features for the desired application from UV to the mid-infrared region [11]. For these reasons, many different fluoride crystals have been investigated in nano-sized shape, such as YF_3, LaF_3, $BaYF_5$, $NaLaF_4$, $NaGaF_4$, and $NaYF_4$ [12-20] with interesting up-conversion emissions and a large interest has been recently devoted to the possibility of enhancing the luminescence efficiency through, for example, the growth of core-shell structures [21,22] or the coupling with plasmon nanostructures [23]. Nevertheless, the choice of the host material is limited by the possibility of obtaining it by chemical synthesis. Many more fluoride crystals are well known as bulk materials, and each of them has peculiar thermo-optical properties that affect the emission features of rare earth dopants. Moreover, very few studies report about the differences in the optical properties of NC compared with the bulk material of the same composition, and in these studies, important differences in the emission spectra are evidenced [24] for which no conclusive explanation has been found, yet. For this reason, it would be extremely desirable to extend this characterization to the whole class of fluoride crystals and, especially, to carry out a comparison of the spectral features of NC and bulk materials of the same composition in order to observe any change that can be induced by the nanometric size.

In this work, we present high-energy ball milling as a simple, versatile, low cost and easily scalable production method that does not involve the handling of toxic or dangerous solvents

or surfactants. High-energy ball milling has already been used for the synthesis of various nanomaterials, nanograins and nano-composites from solid state [25-27], and has also attracted particular interest in the industrial production for various applications such as medical/personal care, batteries, compounds of non-metallic elements and catalysis [28]. With this method we produced 1.25%Pr:BaY_2F_8 (Pr:BYF) NC with an average diameter of 24nm. This top-down approach naturally permits to compare the spectral features of the NC with those of a bulk crystal of the same composition, and gives the unique possibility to study the modifications induced by the nanometric size and get a deeper insight in the physical processes that lead to the extremely interesting fluorescence of these materials. Moreover, BaY_2F_8 crystal is a very good laser host material from which efficient lasing has been obtained in various wavelength regions [29-33], mOreover, it has also proven to be a good material for white light emission [34] and has already been found to be a good emitter in nano-crystalline form when doped with Yb and Er [35]. We performed spectroscopic experiments on nanocrystal samples (NC) and on a bulk crystal (BC) of the same composition at both 10K and room temperature.

2. Experimental details

2.1 Single crystal growth and crystal structure

BYF is a monoclinic crystal with cell parameters a = 6.935Å, b =10.457Å, c = 4.243Å, α = γ=90°, and β=99° 40' [36]. The main symmetry axis is the b-axis with symmetry $C_{2/m}$. The rare-earth ions occupy the Y-site. The point symmetry of the Y lattice site is C_{2h}. A BaY_2F_8 crystal doped with 1.25 at% Pr^{3+} (concentrations in the melt, given with respect to the Y-site) was grown by the Czochralski method. The growth facility consists of a Czochralski furnace with resistive heating and automatic optical diameter-control. Crystal growth was carried out in high-purity argon atmosphere to avoid contamination of the crystal. The starting materials were

proper amounts of 5N fluoride powders supplied by AC materials (Tarpon Springs, FL, USA). The dopant was added to the pure BaY_2F_8 melt in trivalent form (PrF_3), and a proper amount of BaF_2 was added for compensation. The growth process was carried out at temperature around 970°C, with 0.5mm/h pulling rate, and 5rpm rotation rate. The crystal was of good optical quality and free of cracks. It was oriented by X-ray Laue technique, cut along the X,Y,Z optical axes of the crystal and polished to allow polarized measurements. The samples obtained were parallelepipeds with sides in the range 2-8mm.

2.2 Nanocrystal preparation

Crystal pieces were cut from the single crystal boule and used for NC production. This ensures the identical composition of NC and BC. Single crystal pieces were pestled in an agate mortar. Subsequently they were put in a ZrO_2 jar together with water and ZrO_2 spheres and then milled using the Planetary Micro Mill PULVERISETTE 7 premium line (Fritsch GmbH) with 14 cycles at 800RPM for 5min each. Adequate rest time was waited between cycles to allow thermal cooling of the system in order to prevent any temperature-induced chemical modification in the material. Separation of the nanometric component was performed through centrifugation.

2.3 TEM Characterization

Transmission Electron Microscope (TEM) analysis was carried out with Zeiss Libra 120 transmission electron microscope working at 120kV and equipped with an in-column Omega filter. The sample was prepared by dispersion in isopropyl alcohol and, after sonication, a drop of the dispersion was put on a carbon coated copper grid and let evaporate.

2.4 Spectroscopic Characterization

Emission spectra polarized parallel to the X, Y and Z optical axes of the BC sample were measured in order to observe all possible transitions of the Pr^{3+} ion in BYF in the visible range. Polarized measurements were then averaged to obtain unpolarized spectra to be compared with results on NC. We performed measurements both at room and at low (10K) temperature. For the NC samples, the powders were dispersed in methanol, deposited onto a sample holder and let evaporate.

For low temperature measurements, the sample was in thermal contact with the cold finger of a closed-cycle helium cryostat. Particular care was devoted to the quality of the thermal contact and the system was given ample time to equilibrate. The samples were pumped by a diode laser beam with incident power of about 100mW and wavelength of 445nm (energy 22472cm^{-1}), corresponding to the highest absorption peak of Pr^{3+} in the BC [37]. At room temperature, the bulk sample was mounted with the input face either perpendicular to the pump beam or at 45° with respect to it that is, in the same experimental conditions used for the NC, to check if the mounting geometry could induce any relevant difference in the spectra. In all cases, the fluorescence signal was detected perpendicularly to the pump laser direction. The luminescence was then chopped, filtered with a polarizer and focused on the input slit of a 0.25m (at 10K) or 0.33m (at room temperature) monochromator equipped with a 1200grooves/mm grating. The signal was detected by a suitable photomultiplier (S20 cathode) and sent to a lock-in amplifier. Data were recorded by a computer for storage and data analysis purposes. All spectra were normalized for the optical response of the system using a black body source at 3000K. In spite of the monchromator filtering, NC spectra showed a strong residual scattering from the laser line in the short-wavelength part of the spectrum. This scattering was subtracted from the acquired spectra with a phenomenological fit of the fourth or sixth power of the inverse of the

wavelength difference from the laser line (445nm). This procedure yielded a good elimination of the background scattering.

For the lifetime measurements the apparatus was similar, but the pump source was a pulsed doubled Ti:Sapphire laser (30ns pulse duration, 10Hz repetition rate) tuned to the maximum absorption of the sample around 22000cm^{-1} and the luminescence was filtered with suitable filters. The amplification chain was properly modified and the signal was sent to a digital oscilloscope and then stored on a PC. The response time of the detection apparatus was 1μs.

3. Experimental results and discussion

3.1 TEM characterization

Figure 1a shows an example of the bright field TEM images used for the analysis. The statistical analysis was carried out on 533 nanoparticles.

NCs showed irregular shapes with limited asymmetry. Figure 1b shows the statistical distribution of the measured diameters. The average grain size is 24nm with a standard deviation of 8nm and the median is 22nm. The minimum diameter measured is 7.5nm and the largest is 56nm. Since this wide particle size distribution has been obtained with standard centrifugation technique, we believe that a careful optimization of the procedure or the use of more sophisticated techniques could lead to a narrower distribution.

3.2 Photoluminescence spectra

Figure 2 shows the unpolarized luminescence of the BC and NC samples in the visible range (450–750nm) at 10K. For the BC sample the unpolarized spectrum was obtained as an average over the three possible polarizations and the NC spectrum has been multiplied by a factor of 6

and shifted for better readability. The spectra contain lines originating from the $^3P_0$, $^3P_1$, $^3P_2$ $^1D_2$ and $^1I_6$ levels and the number of observed lines never exceeds the number of theoretical lines predicted, as expected in samples of good crystal quality. Moreover, no significant differences in the energy position and line width of the two samples are observed. This implies that no substantial structural changes are induced in the sample during the high-energy milling process, that is, the NC retain the good crystalline quality of the bulk sample. This demonstrates that the high-energy milling method is capable of producing high quality NC with size less than 25nm and that the number of ions residing in sites so close to the surface to see a distorted symmetry that modifies the energy level positions is negligible. It may be worth noting that the starting material could also be a polycrystalline mass, rather than a Czochralski-grown single crystal, in fact, the single crystal has been pestled before the milling process, and this makes the method even more versatile.

Although the shapes of the emission bands are similar in both BC and NC samples, there are noticeable changes in their intensities. Regarding the overall luminescence of NC in comparison to the BC sample (excited at the same pump level), it should be noted that in Figure 2 the NC spectrum has been amplified by a factor of 6. It is generally believed that nanoparticles have smaller luminescence efficiency than their bulk counterparts due to the large surface area in which a variety of quenchers can exist [38]. Moreover, also upconversion is believed to be less efficient in NC [22] even if its efficiency has shown anomalous behavior in some cases [39]. However, it is difficult or even misleading, to compare the absolute emission intensity of different samples. In spite of the identical experimental setup and pump level, such differences can be connected to the lower density of the NC powder with respect to the bulk samples, to different observed volumes, or any other experimental differences in the setups, but also to a different average refractive index of the surrounding medium and to trapping effects [40,41].

Much more informative are the differences in the relative intensity of the various lines, which are expected to be identical in the two samples. On the contrary, in our case some lines appear much more intense in the NP and others much weaker. In other words, we observe a redistribution of the emitted energies over the different emission lines. In fact, a few lines are present in one of the samples and not in the other. One line of the $^3P_0 \rightarrow {}^3F_3$ transition is not present in the NC spectrum ($\lambda \approx 14129 cm^{-1}$), but this line is very weak in the BC sample, too. What is more striking is that the whole $^1D_2 \rightarrow {}^3H_4$ transition is clearly visible in the NC, but is completely missing in the BC sample. In general, the lines belonging to different transitions show different relative intensity in the two samples, in particular the $^3P_0 \rightarrow {}^3H_4$ and $^1D_2 \rightarrow {}^3H_4$ transitions appear to be hyper intense in the NC, in fact their intensity is much higher in NC than in BC even after correcting for the factor of 6 amplification in the figure. On the other hand, the other transitions, including those originating from $^3P_0$, and $^1D_2$ are generally weaker in NC. This seems to be connected to differences in the oscillator strengths in the two samples rather than to different populations of the emitting levels. In fact, the lines originating from the same level but arriving to different levels have different relative intensities in the two samples. Moreover, the intensity ratios of the different lines in the NC over the BC do not seem to have a simple dependence on the energy of the emitted photons, therefore, a phenomenon linked to different photon modes in the nanoparticles with respect to the bulk sample (which could affect the spontaneous emission ratio) should be ruled out. Instead, there seems to be a strong dependence on the final state of the ion, being the transitions towards higher (lower) states the most depressed (amplified).

In order to have a better picture of the situation we also compared the room temperature emission spectra of the two samples. Figure 3 shows the room temperature unpolarized

emission spectra. The NC spectrum has been multiplied by a factor of 3 and shifted for better readability. The room temperature spectra confirm the 10K observations: the peak positions and widths are identical in the two samples, the overall luminescence intensity is lower in the NC, but some transitions appear to be hyper intense in the NC. A closer look to the spectra indicate that, for every emitting level, the relative intensity of the NC emission tend to diminish with decreasing the energy of the transition. Similarly to the low temperature emissions, the transitions of $^3P_0$ and $^1D_2$ to the fundamental $^3H_4$ are more intense in the NC, while the transitions to the excited levels ($^3H_5$, $^3H_6$, $^3F_2$, $^3F_3$, $^3F_4$) are less intense in the NC. The $^3P_2$ level shows three transitions in the visible spectral range: referring to the arbitrary scale used in figure 3, one notices that the $^3P_2 \rightarrow {}^3H_5$ transition is more intense in the NC, $^3P_2 \rightarrow {}^3H_6$ has comparable intensity, and $^3P_2 \rightarrow {}^3F_2$ is less intense. To visualize this trend, we calculated the intensity ratio between the NP and bulk fluorescence of the lines we could unambiguously assign and plotted it against the energy of the final level of the transition. This result is summarized in Figure 4 where the solid line is just a guide for the eye. With this analysis, any difference in the quantity of analyzed sample (*e.g.* caused by the amount of NC used, the size of the BC, a different geometry in the setup) is cancelled out in the ratio, and the result should be constant if all the physical processes leading to the emissions were the same in BC and NC. Instead, the intensity ratio decreases with the energy of the final level and the trend is similar for various emitting levels both at room temperature and 10K. Again, this cannot be explained with a different population of the emitting levels in the two samples or to the different method used for averaging over the polarizations, instead it confirms that the nanometric size of the samples favors the transitions towards the lower energy states over the higher ones. Unfortunately, due to the overlapping of different transitions, it was not possible to extract a clear quantitative trend in the emission intensity of the various lines, and more investigations

are needed in this respect, even with other active ion doping and/or other host materials. It is generally believed that the fluorescence in nano-sized materials is usually quenched by external centers that interact with the NC surface, but this would affect the overall population of the emitting levels and therefore, all transitions originating from the same multiplet should be equally quenched. Possible explanations, instead, could be connected to a surface modification of the density-of-states of phonons that produce changes in the nonradiative relaxation rates in nanoparticles [42], to a different electron-phonon coupling of Pr ions residing near the surface [10] or to a slight difference of the crystal potential for these same ions, which could be small enough to prevent observable changes of the energies of the transitions but could affect the dipole elements between the different states. It should be noted, in fact, that most of the observed transitions are not allowed in a dipole approximation for the free ions, and even a really small mixing could affect the oscillator strengths. Presently, we have no conclusive explanation for these behaviour and its theoretical study is beyond the aim of this manuscript, moreover, more detailed analysis of the differences between NC and BC of this or other compounds with a simpler energy level scheme will be necessary to have a complete picture of the situation.

Fluorescence decay analysis

The room temperature decay curve of the blue $^3P_0 \rightarrow {}^3H_4$ fluorescence of Pr^{3+} ions in BaY_2F_8 BC and NC are shown in Figure 5 in semi-logarithmic scale. The linear relationship of the BC decay demonstrates its single exponential character. The fluorescence lifetime of the $^3P_0$ manifold in BYF:Pr^{3+} BC is obtained by linear fitting of the results and it is $\tau = 43\mu s$. This is

comparable to the radiative lifetime $(\tau_{rad} = 49\mu s)$ of this manifold calculated previously from the JO theory at room temperature [37].

The luminescence quantum efficiency (η) is defined as the ratio of the number of photons emitted to the number of photons absorbed and is equal to the ratio of the experimental lifetime to the predicted radiative lifetime and it is given by:

$$\eta = \frac{\tau_{\exp}}{\tau_r} * 100 \qquad (1)$$

The η value for the $^3P_0$ level at room temperature is found to be 88% for BaY_2F_8 BC. This high quantum efficiency of the $^3P_0$ visible emission suggests BaY_2F_8 crystal as a potential host material for various applications.

Room temperature fluorescence decay curve of the $^3P_0$ multiplet of Pr:BYF NC, shows a strongly non-exponential character. The difference between NC and BC decay is striking, but the difference is not simply a longer or shorter exponential decay, as predicted for example in [40], but a strong deviation from the linear character. This could be due to the presence of quenching centers at the NC surface, or to the fact that bilinear processes play a much different role in NC and in BC. It is well known that Pr ions excited in the ^3P_j levels can undergo different cross relaxation processes, such as $(^3P_{0,1}, {}^3H_4) \rightarrow (^3H_6, {}^1D_2)$ and/or $(^3P_{0,1}, {}^3H_4) \rightarrow (^1G_4, {}^1G_4)$, [43] even if we did not observe strong evidence in the BC, probably due to the low doping level of the material.

Under certain assumptions Inokuti and Hirayama [44] developed a model for bilinear decays which assumes that the energy of an excited donor transfers to the surrounding acceptors in the

ground state directly and gives the possibility to determine the nature of ion–ion interaction (dipole–dipole D–D, dipole–quadrupole D–Q or quadrupole–quadrupole Q–Q). If the process responsible for the non-exponential decay is cross-relaxation, the expression derived by Inokuti and Hirayama for the decay of luminescence of a donor–acceptor system is given by:

$$I(t) = I(0)\exp\left[-\frac{t}{\tau_0} - \Gamma\left(1-\frac{3}{S}\right)\frac{N_A}{N_c}\left(\frac{t}{\tau_0}\right)^{3/S}\right] \qquad (2)$$

where τ_0 is the intrinsic lifetime of the donor, Γ is the Euler gamma function, which is equal to 1.77 for dipole–dipole (S = 6), 1.43 for dipole–quadrupole (S = 8) and 1.3 for quadrupole–quadrupole (S = 10) interactions, respectively. N_A is the acceptor concentration, and N_c is a critical transfer concentration.

For S = 6 one obtains

$$N_c = \frac{3}{4\pi R_0^3} \qquad (3)$$

where R_0 is the critical transfer distance defined as the donor–acceptor separation for which the rate of energy transfer between a donor and acceptor is equal to the rate of intrinsic decay rate (τ_0^{-1}) of the donor. The dipole– dipole interaction parameter C_{DA} is related to R_0 as:

$$C_{DA} = \frac{R_0^6}{\tau_0} \qquad (4)$$

The above expression becomes

$$I(\mathrm{t}) = \mathrm{I}(0)\exp\left(-\frac{t}{\tau_0} - \gamma\sqrt{t}\right), \qquad (5)$$

$$\gamma = \frac{4}{3}\pi^{3/2} N_A \sqrt{C_{DA}} \qquad (6)$$

In Figure 6 the NC fluorescence decay curve of the $^3P_0 \rightarrow {}^3H_4$ transition is plotted as $\ln(\mathrm{I(t)/I_0}) + t/\tau_0$ against $(t/\tau_0)^{3/S}$ for S=6, 8, and 10 together with the best linear fitting based on the Inokuti–Hirayama model. From Fig. 6 it is clear that none of the functions used for fitting is able to reproduce the experimental decays, in fact the experimental data are not represented by a straight line in the $\ln(\mathrm{I(t)/I_0}) + t/\tau_0$ - $(t/\tau_0)^{3/S}$ space.

The failure of the Inokuti–Hirayama model indicates that our physical conditions do not fulfill the assumptions of the model. One of these is that the number of excited ions must be small compared with the total number of active ions. It is worth noting that the BC of the same composition and in the same experimental conditions shows an exponential decay, and this means that the doping concentration and the excitation density in this case are small enough not to trigger bilinear processes.

Time dependence of the $^3P_0$ luminescence intensity for higher concentrations could also be explained using the diffusion limited energy transfer model proposed by Yokota and Tanimoto [45]. This model describes the decay of the donor luminescence in bulk materials, but its application to nano-objects is questionable because in this model, diffusion within the donor network is supposed to occur before a donor transfers its excitation energy to an acceptor nearby. In a nano-object a diffusion process over large distances is unlikely to occur because the excitation cannot cross the grain boundaries. Furthermore, the shape of the nanoparticles

(spherical, ellipsoidal. . .) can influence the decay profile as discussed in [46]; therefore, we did not apply this model to our system.

We have found however that the temporal behavior of the $^3P_0$ level can be modelled by a simple bi-exponential decay, as sometimes found with other Pr-doped compounds [47-50]:

$$I(t) = A_1 \exp(\frac{-t}{\tau_1}) + A_2 \exp(\frac{-t}{\tau_2}) \qquad (7)$$

where τ_1 and τ_2 are the slow and fast decay components (long and short lifetimes), A_1, A_2 are the fitting weighing factor parameters. The best fitting for NC is shown in figure 7. The agreement with experimental data, in this case, is very good and the parameters obtained are $A_1 = 0.89$, $\tau_1 = 2.45\mu s$, $A_2 = 0.11$, $\tau_2 = 26.7\mu s$. The fast decay is attributed to the presence of a strong quenching mechanism and the slow decay is of the same order, but shorter than BC lifetime. This can be caused by the fact that there could actually be a continuous distribution of fluorescent decay times, that is however well represented by a simple bimodal one, with contributions to the slower population given also by slightly perturbed Pr^{3+} ions. In any case, in terms of τ_1, τ_2, A_1 and A_2, it is possible to distinguish the number of ions decaying with different lifetimes. The percentage of ions (N) with fast lifetime τ_1 is given by:

$$N = \frac{A_1}{A_1 + A_2} \qquad (8)$$

The calculated values of N, with the above equation is 89% for 1.25% Pr^{3+} doped BaY_2F_8. Since the usual models for non-linear energy transfer processes did not satisfactorily fit the decay kinetics, and because of the fact that the decay was linear in BC, we attribute the fast decay component to surface effects of ions residing near the surface of the NP.

Using the above two lifetime values (τ_1 and τ_2), the amplitude average lifetime $\langle\tau\rangle$ have been calculated for Pr^{3+} emission states from:

$$\langle\tau\rangle = \frac{A_1\tau_1 + A_2\tau_2}{A_1 + A_2} \quad \textbf{(9)}$$

The average lifetime of Pr^{3+}:BaYF NC (τ_{exp}) is found to be 5.1μs. The luminescence efficiency calculated with (1) in this case is η =10.4%. Both the average lifetime and the luminescence efficiency are, therefore, much smaller in NC than in BC.

Conclusions

We used the high-energy ball milling process to produce 1.25% Pr:BaY_2F_8 nanocrystals with average diameter of 24nm. The method is simple, versatile, low cost and easily scalable. In fact, it can also be applied starting from a polycrystalline mass or powder instead of a Chzochralski-grown single crystal. Moreover, it naturally permits a comparison of the emission properties of bulk material and NC to have a deeper insight in the physical processes taking place in nano-sized materials. In fact, we compared the fluorescence features of NC and bulk crystal of the same composition. The 10K and room temperature luminescence did not show any relevant difference in the peak position and width. This demonstrates that the milling process did not induce any structural modification in the crystal quality. The main differences between BC and NC regards the relative intensities of the various emission lines, and the temporal behavior of the luminescence. A detailed analysis of the 10K and room temperature emission intensity of the various lines shows that transitions to the ground state appeared to be hyper intense in the NC, but transitions to excited states tend to weaken with increasing the energy of the final level. Therefore, the nanometric size of the grains have an influence on the various transition probabilities probably due to a surface modification of the density-of-states of phonons that

produce changes in the nonradiative relaxation rates or to differences in the crystal potential for these same ions, which could affect the dipole elements between the different states. Another striking difference between the two samples regards the temporal behavior of the $^3P_0$ emitting level: the decay is exponential in the bulk material, but strongly non exponential in the NC. About 89% of the active ions seem to contribute to the short-decay-time behavior, that is, atoms that should be placed near the NC surface at a distance small enough to feel surface effects.

Acknowledgements

The authors thank Daniela Parisi and Ilaria Grassini for help in the preparation of the bulk sample.

References

[1] Shalav, A.; Richards, B. S.; Trupke, T.; Kramer, K.W.H.; Gudel, U. Application of $NaYF_4:Er^{3+}$ Up-converting Phosphors for Enhanced Near-infrared Silicon Solar Cell Response. *App. Phys. Lett* .**2005**, 86, 013505/1-3.

[2] Bünzli, J.-C. G.; Eliseeva S, V.; Lanthanide NIR Luminescence for Telecommunications, Bioanalyses and Solar Energy Conversion. *J. of rare earth*, **2010**, 28, 824-842.

[3] Xu, L.; Zhang, S.; Xu, J. Optical Amplification in $NaYF_4$: Nd Nanoparticle Dispersed Solution with Gain. *Laser .Phys. Lett.* **2010**, 7, 303-306.

[4] Wei, Y.; Lu, F.; Zhang, X.; Chen, D.; Synthesis and Characterization of Efficient Near-infrared Upconversion Yb and Tm Codoped $NaYF_4$ Nanocrystal Reporter. *J.of alloys and compounds*, **2007**,427, 333-340

[5] Lim, S. F.; Riehn ,R.; Ryu, W. S.; Khanarian, N.; Tung ,C. K.; Tank, D; Austin, R. H. In Vivo and Scanning Electron Microscopy Imaging of Upconverting Nanophosphors in Caenorhabditis elegans. *Nano Lett.* **2006**, 6, 169-174.

[6] Jalil, R. A.; Zhang, Y. Biocompatibility of Silica Coated $NaYF_4$ Upconversion Fluorescent Nanocrystals. *Biomaterials* **2008,** 29, 4122-4128.

[7] Van de Rijke, F.; Zijlmans ,H.; Vail, S. Li, T.; Raap, A. K.; Niedbala ,R. S.; Tanke, H. J.; Up-converting Phosphor Reporters for Nucleic Acid Microarrays. *Nature biotechnology*, **2001,** 19, 273-276.

[8] Vetrone, F.; Capobianco ,J. A.; Lanthanide-doped Fluoride Nanoparticles: Luminescence, Upconversion, and Biological Applications. *Int. J .Nanotechnol.* **2008**, 5, 1306-1339.

[9] Haase, M.; Schafer, H.; Upconverting Nanoparticles. *Angew. Chem. Int. Ed.* **2011**, 50, 5808-5829.

[10] Tissue, B. M.; Synthesis and Luminescence of Lanthanide Ions in Nanoscale Insulating Hosts. *Chem. Mater.* **1998**, 10, 2837-2845.

[11] Wang, F.; Liu, X. Upconversion Multicolor Fine-tuning: Visible to Near-Infrared Emission from Lanthanide-doped NaYF4 Nanoparticles. *Journal of the American Chemical Society* **2008**, 130, 5642-5643.

[12] Pellè, F.; Dhaouadi ,M.; Michely, L.; Aschehoug, P.; Toncelli ,A.; Tonelli ,M.; Veronesi, S. Spectroscopic Properties and Upconversion in Pr^{3+}:YF_3 Nanoparticles. *Phys. Chem. Chem. Phys.* **2011**, 13, 17453-17460.

[13] Yu, X.; Li ,M.; Xie, M.; Chen, L.; Li,Y.; Wang ,Q. Dopant-controlled sSynthesis of Water-Soluble Hexagonal $NaYF_4$ Nanorods with Efficient Upconversion Fluorescence for Multicolor Bioimaging. *Nano Res.* **2010**, 3, 51-60.

[14] Wang, L.; Zhang , Y. ; Zhu, Y. One-pot Synthesis and Strong Near-infrared Upconversion Luminescence of Poly (acrylic acid)-functionalized YF_3: Yb^{3+}/Er^{3+} Nanocrystals *Nano Res.* **2010**, 3, 317-325.

[15] Sun, J.; Xian, J.; Xia, Z.; Du, H. Synthesis of Well Oil-dispersible $BaYF_5$:Yb^{3+}/Er^{3+} Nanocrystals with Green Upconversion Fluorescence . *J. Rare Earths* **2010**, 28, 219-221.

[16] Yi, G.; Lu, H.; Zhao, S.; Ge, Y.; Yang, W.; Chen, D.; Guo, L.H. Synthesis, Characterization, and Biological Application of Size-controlled Nanocrystalline $NaYF_4$: Yb, Er Infrared-to-visible Up-conversion Phosphors. *Nano Lett.* **2004**, 4, 2191-2196.

[17] Yan, R.; Li ,Y. Down/Up Conversion in Ln^{3+}-Doped YF_3 Nanocrystals. *Adv. Funct. Mater*. **2005**, 15, 763-770.

[18] Heer, S.; Kompe, K.; Gudel, H.U; Haase, M. Highly Efficient Multicolour Upconversion Emission in Transparent Colloids of Lanthanide-doped $NaYF_4$ Nanocrystals. *Adv. Mater*. **2004**, 16, 2102-2105.

[19] Mai, H. X.; Zhang, Y. W.; Si, R.; Yan, Z. G.; Sun, L. D.; You, L. P.; Yan, C. H. High-quality Sodium Rare-earth Fluoride Nanocrystals: Controlled Synthesis and Optical Properties. *J. Am. Chem. Soc.* **2006,** 128, 6426-6436.

[20] Gao, L.; Ge, X.; Chai, Z.; Xu, G.; Wang, X.; Wang, C. Shape-controlled Synthesis of Octahedral α-$NaYF_4$ and its Rare Earth Doped Submicrometer Particles in Acetic Acid. *Nano Res.* **2009**, 2, 565-574.

[21] Johnson N. J. J., van Veggel F. C. J. M. Sodium lanthanide fluoride core–shell nanocrystals: A general perspective on epitaxial shell growth *Nano Res.* **2013**, 6, 547–561.

[22] Chen, X., Peng, D., Jua, Q., Wang, F. Photon upconversion in core–shell nanoparticles Chem. Soc. Rev. DOI: 10.1039/c4cs00151f

[23] Xu, W., Zhu, Y., Chen, X., Wang, J., Tao, L., Xu, S., Liu, T., Song, H. A novel strategy for improving upconversion luminescence of $NaYF_4$:Yb, Er nanocrystals by coupling with hybrids of silver plasmon nanostructures and poly(methyl methacrylate) photonic crystals *Nano Res.* **2013**, 6, 795–807.

[24] Capobianco, J. A.; Vetrone, F.; D'Alesio, T.; Tessari, G.; Speghini, A.; Bettinelli, M. Optical Spectroscopy of Nanocrystalline Cubic Y_2O_3: Er^{3+} Obtained by Combustion Synthesis. *Phys. Chem. Chem. Phys.* **2000**, 2, 3203-3207.

[25] Matteazzi, P.; Alcala , M. Mechanomaking of Fe/Al_2O_3 and $FeCr/Al_2O_3$ Nanocomposites Powders Fabrication. *Material Science and Engineering A.* **1997,** 230, 161-170.

[26] Zhang ,D.L. Processing of Advanced Materials Using High-energy Mechanical Milling *Progress in Materials Science.* **2004**, 49, 537-560.

[27] Akdogan, N. G.; Hadjipanayis, G. C.; Sellmyer,D. J. Novel Nd(2)Fe(14)B Nanoflakes and Nanoparticles for the Development of High Energy Nanocomposite Magnets . *Nanotechnology* **2010,** 21, 295705/1-5.

[28] James, S. L., Adams, C. J., Bolm, C., Braga, D., Collier, P., Friscic, T., Grepioni, F., Harris, K. D. M., Hyett, G., Jones, W., Krebs, A., Mack, J., Maini, L., Orpen, A. G., Parkin, I. P., Shearouse, W. C., Steedk J. W., Waddelli D. C. Mechanochemistry: opportunities for new and cleaner synthesis *Chem. Soc. Rev.*, **2012**, 41, 413–447.

[29] Agnesi, A.; Guandalini, A.; Tomaselli, A.; Sani ,E.; Toncelli, A.; Tonelli, M. Diode-pumped Passively Mode-locked and Passively Stabilized Nd^{3+}:BaY_2F_8 Laser .*Opt. Lett*. **2004**, 29, 1638-1640.

[30] Coluccelli, N.; Galzerano, G.; Parisi, D.; Toncelli, A.; Tonelli, M.; Laporta, P. Room-temperature Q-switched Tm:BaY_2F_8 Laser Pumped by CW Diode Laser. *Opt. Exp*. **2006**, 14, 1518-1523.

[31] Cornacchia, F.; Parisi, D.; Bernardini, C.; Toncelli, A.; Tonelli, M. Efficient, Diode-pumped Tm^{3+}:BaY_2F_8 Vibronic Laser. *Opt. Exp*. **2004**, 12, 1982-1989.

[32] Gatti, D.; Galzerano, G.; Toncelli, A.; Tonelli, M.; Laporta, P. Actively Mode-locked Tm-Ho:$LiYF_4$ and Tm-Ho:BaY_2F_8 Lasers. *Appl. Phys. B* **2007**, 86, 269-273.

[33] Agnesi ,A.; Pizio, F.; Reali, G.; Toncelli, A.; Tonelli ,M.; Jenssen, H.P. Diode Pumped Nd:BaY_2F_8 Picosecond Laser . *Opt. Commun*. **2008**, 281, 6094-6096.

[34] Toncelli, A.; Bonelli, L.; Faoro, R.; Parisi, D.; Tonelli, M., Investigation of Pr-doped Fluoride Crystals as Possible White-light Emitters .*Optical Materials* **2009**, 31, 1205-1209.

[35] Wang, G., Peng Q., Li, Y. Synthesis and upconversion luminescence of $BaY_2F_8:Yb^{3+}/Er^{3+}$ nanobelts *Chem. Commun*., **2010**, 46, 7528–7529.

[36] Toncelli, A., Tonelli, M., Cassanho, A., Jenssen, H. P. Spectroscopy and dynamic measurements of a Tm,Dy:BaY2F8 crystal *Journ. Lumin*. **1999**, 82, 291-298

[37] Hakim. R.; Damak. K.; Toncelli. A.; Fourati. M. ;and Maalej. R. Growth, Optical Spectroscopy and Judd–Ofelt Analysis of Pr-doped BaY_2F_8 Monocrystals. *J. Lumin.* **2013**, 143, 233-240.

[38] Dai, Q.; Song, H.; Pan, G.; Bai, X.; Zhang, H.; Qin, R.; Hu, L.; Zhao, H.; Lu, S.; Ren, X. Surface Defects and Their Influence on Structural and Photoluminescence Properties of $CdWO_4:Eu^{3+}$ Nanocrystals .*J. Appl. Phys*. **2007**, 102, 054311-8.

[39] Chen ,G. Y.; Liang, H. J.; Liu, H. C.; Somesfalean, G.; Zhang, Z. G. Anomalous Power Dependence of Upconversion Emissions in Gd_2O_3: Er^{3+} Nanocrystals Under Diode Laser Excitation of 970 nm. *J. Appl. Phys.* **2009**, 105, 114315/1-5.

[40] Meltzer. R. S.; Feofilov. S. P.; Tissue. B.; Yuan. H. B. Dependence of Fluorescence Lifetimes of $Y_2O_3:Eu^{3+}$ Nanoparticles on the Surrounding Medium .*Phys. Rev. B* **1999**, 60, R14012-R14015.

[41] Toncelli. A.; Ahmadi. B.; and Marchetti. F.; Upconversion Enhancement in Yb^{3+},$Tm^{3+}:BaY_2F_8$ Quasi-nanoparticles. *Journ. Lumin*. **2012**, 132, 2268-2274.

[42] Wolf. D.; Wang. J.; Phillpot. S. R.; and Gleiter. H. Phonon-Induced Anomalous Specific Heat of a Nanocrystalline Model Material by Computer Simulation . *Phys. Rev. Lett.* **1995,** 74, 4686-4689.

[43] Sokolska. I.; Gołab. S.; Bałuka. M.; and Ryba-Romanowski .W. Quenching of Pr^{3+} Emission in Single Crystals of $K_5Pr_xLa_{1-x}Li_2F_{10}$. *J. Lumin.* **2000**, 91, 79-86.

[44] Inokuti. M.; and Hirayama. F. Influence of Energy Transfer by the Exchange Mechanism on Donor Luminescence *J. Chem. Phys.* **1965**, 43, 1978-1989.

[45] Yokota. M.; and Tanimoto. I. Effect of Diffusion on Energy Transfer by Resonance *J. Phys. Soc. Jpn.* **1967**, 22, 779-784.

[46] Basiev. T.; Orlovskii. Y.; and Pukhov. K. Spontaneous and Induced Emission in Dielectric Nanoparticles . *Nanotechnol. Russ.*, **2008**, 3, 551-559.

[47] Diallo, P. T., Boutinaud, P., Mahiou, R. Anti-Stokes luminescence and site selectivity in $La_2Ti_2O_7:Pr^{3+}$ *J. Alloys and Compd.* **2002**, 341, 139–143.

[48] Jia, G., Wang, H., Lu, X., You, Z., Li, J., Zhu, Z., Tu, C. Optical properties of Pr^{3+}-doped $SrWO_4$ crystal *Appl. Phys. B* **2008**, 90, 497–502.

[49] Wang, Y., Li, J., You, Z., Zhu, Z., Tu, C. Spectroscopic properties of $Pr^{3+}:Gd_3Ga_5O_{12}$ crystal *J. Alloys and Compd.* **2010**, 502, 184–189.

[50] Wei, Y., You, Z., Ma, X., Li, J., Zhu, Z., Wang, Y., Tu, C., Optical properties of Pr^{3+}: $NaLa(WO_4)_2$ single crystal J. Phys. D: Appl. Phys. **2008**, 41, 165404/1-6.

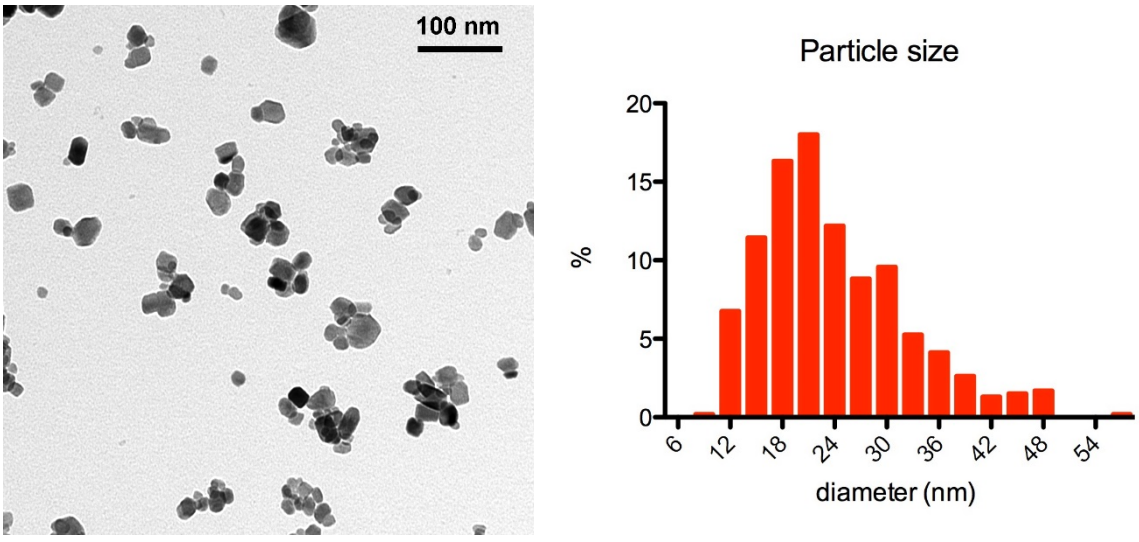

a) b)

Figure 1: a) TEM bright field image of a dispersion of Nps. b) Plot of the grain size distribution

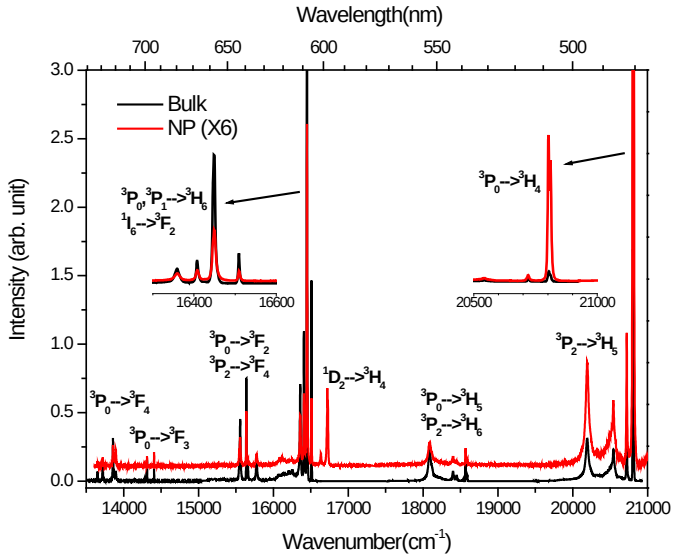

Figure 2: 10K fluorescence of Pr^{3+}:BaY_2F_8 crystal and NC.

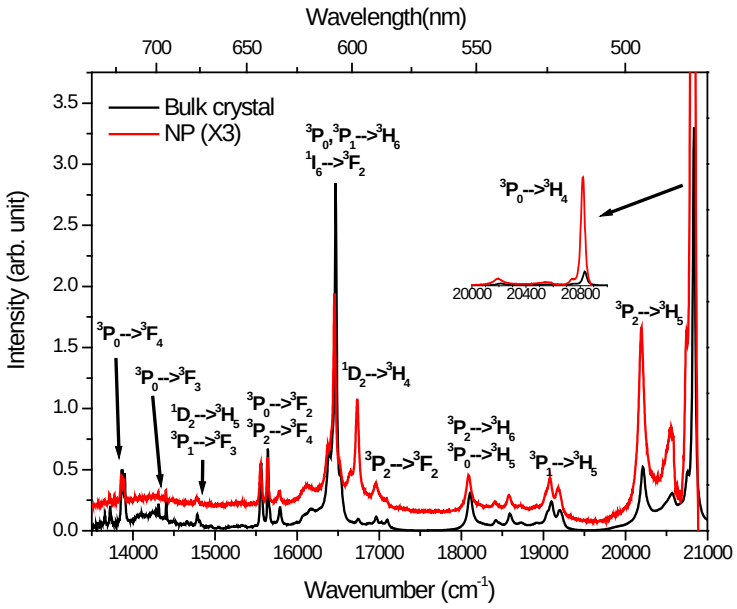

Figure 3: Room temperature emission spectra of 1.25% Pr:BaYF NC and bulk crystal.

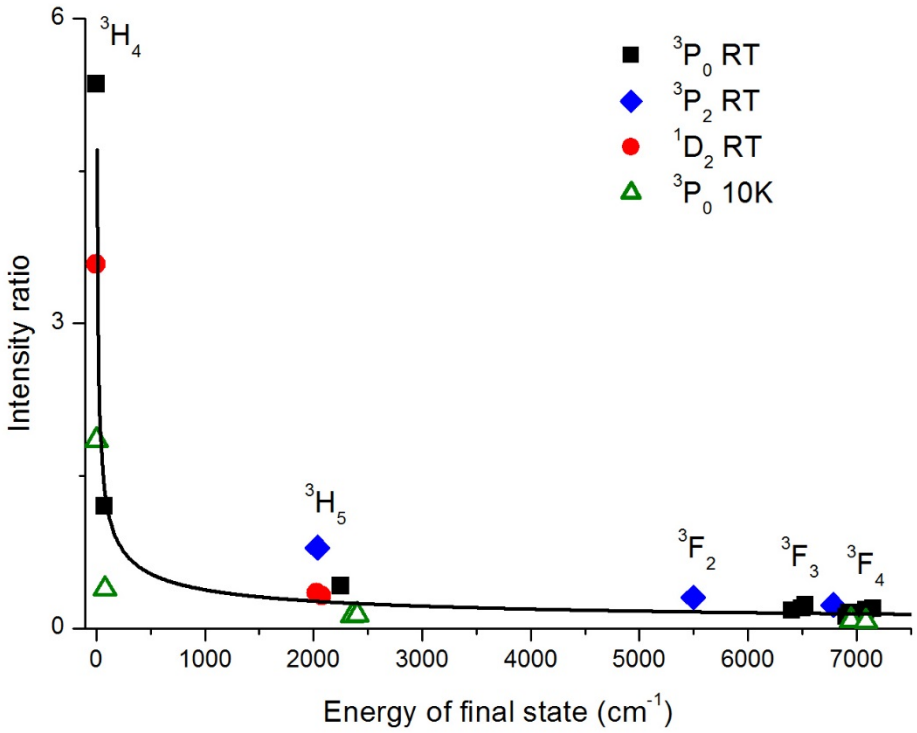

Figure 4: Intensity ratio of the various emitting lines of 1.25% Pr:BaYF NC and bulk crystal plotted as a function of the energy of the final state of the transition. The legend shows the emitting level, the graph the assignment to the final multiplets.

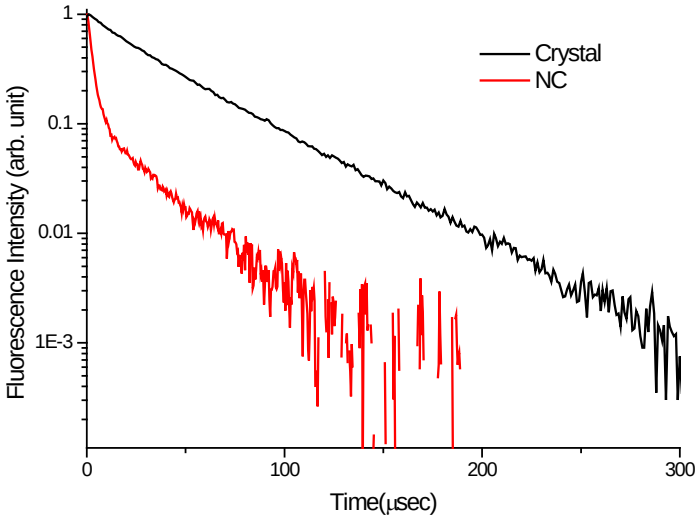

Figure 5: Room-temperature fluorescence decay curves of NC and crystal.

S=6 (a) **S=10** (c)

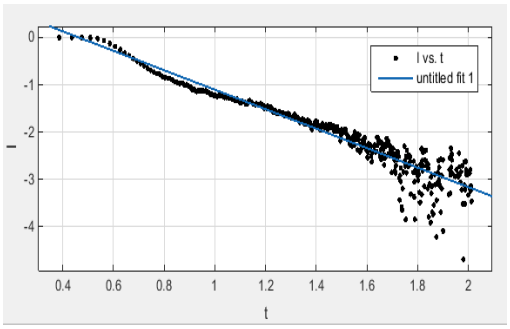

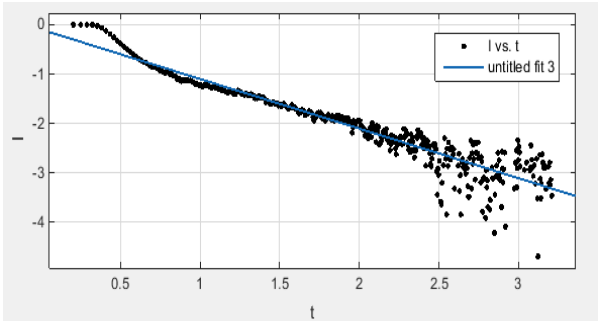

S=8 (b)

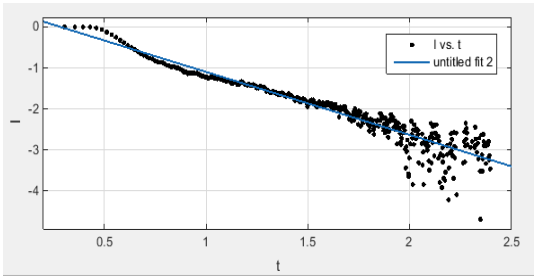

Figure 6: Inokuti–Hirayama presentations with (a) *s* = 6, (b) *s* = 8, and (c) *s* = 10 of the room-temperature fluorescence decay curve for the $^3P_0 \rightarrow {}^3H_4$ transition of Pr^{3+}:BaY_2F_8 nanocrystal. The *points* represent the experimental results by plotting ln [*I(t)/I*(0)]+*t*/*τ*0 against *(t/τ*0*)*3/*s* and the *solid lines* represent the Inokuti–Hirayama fits.

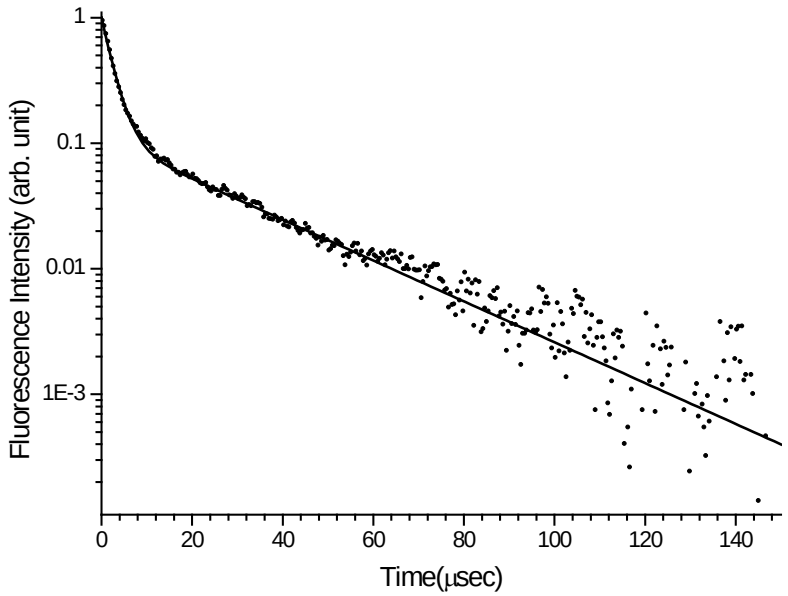

Figure 7: Room-temperature fluorescence decay curve of Pr^{3+}:BaY_2F_8 crystal with bi-exponential fit (solid line) superimposed.